

## Supporting Information:

# Excited state mechanisms in crystalline carbazole: the role of aggregation and isomeric defects

Federico J. Hernández and Rachel Crespo-Otero\*

*Department of Chemistry, School of Biological and Chemical Sciences, Queen Mary  
University of London, London, UK*

E-mail: r.crespo-otero@qmul.ac.uk

## Contents

<b>S1 Gas Phase</b>	<b>S2</b>
S1.1 Orbitals and electronic density differences for the monomer in the gas phase	S6
<b>S2 Marcus-Levich-Jortner rate for electron transfer processes</b>	<b>S7</b>
<b>S3 Comparison between embedded cluster models</b>	<b>S9</b>
<b>S4 Calculation of fluorescence time constant and quantum yields</b>	<b>S10</b>
<b>S5 The centred molecule mechanism of pure Cz crystal</b>	<b>S11</b>
S5.1 Spectroscopic characterization . . . . .	S11
S5.2 ISC mechanism from S <sub>2</sub> . . . . .	S12
S5.3 S <sub>2</sub> /S <sub>1</sub> and T <sub>3</sub> /T <sub>2</sub> crossing geometries . . . . .	S13

S5.4 Spin-Orbit coupling values for an embedded molecule . . . . .	S14
<b>S6 Huang-Rhys factors</b>	<b>S14</b>
<b>S7 Carbazole Dimers</b>	<b>S15</b>
S7.1 Dimer Structures . . . . .	S15
S7.2 Transition Densities . . . . .	S16
S7.3 Energies and spin-orbit couplings for the embedded dimers . . . . .	S17
S7.4 Phosphorescence from Cz dimers . . . . .	S17
S7.5 Exciton transport in the triplet manifold . . . . .	S19
S7.6 $S_{0\min}$ Dimer Coordinates . . . . .	S20
<b>S8 HOMO and LUMO energies</b>	<b>S22</b>
<b>S9 Bd-Cz dimers</b>	<b>S22</b>
S9.1 Dimer A . . . . .	S22
S9.1.1 Effect of long-range electrostatic interactions . . . . .	S22
S9.1.2 ADC(2) energies of dimer A . . . . .	S23
S9.2 Dimer B . . . . .	S25
S9.3 Dimer C . . . . .	S26
<b>S10 Cz<sup>-</sup> absorption transitions</b>	<b>S27</b>

## S1 Gas Phase

The molecule of Cz was optimised in vacuum in the  $S_0$ ,  $S_1$ ,  $S_2$  and  $T_1$  states considering the (TD-)DFT and ADC(2) methods. At the (TD-)DFT level, the global hybrid functionals PBE0,  $\omega$ HPBE0, BLYP and B3LYP, and the long-range corrected hybrid functionals LC-PBE0, LC- $\omega$ HPBE0, LC-BLYP, CAM-B3LYP and  $\omega$ B97XD were used with the Pople's basis sets 6-31+G(d) and 6-311++G(d,p). For the ADC(2) calculations, the Karlsruhe's basis set

def2-TZVP was used instead. All the (TD-)DFT calculations were performed with Gaussian 16,<sup>S1</sup> whereas the ADC(2) calculations were done with Turbomole.<sup>S2</sup>

The long-range corrected functionals were optimised by tuning the range-separation parameter  $\gamma$  that splits the exchange term into the short-range and long-range terms. The following objective function was optimised,<sup>S3,S4</sup>

$$J^2(\gamma) = [\epsilon_{HOMO}^\gamma(N) + IP^\gamma(N)]^2 + [\epsilon_{HOMO}^\gamma(N+1) + IP^\gamma(N+1)]^2, \quad (\text{S1})$$

where  $\epsilon_{HOMO}^\gamma(N)$  represents the HOMO of the N-electron system, and  $IP^\gamma(N)$  stands for the energy difference between the ground-state energies of the N and N-1 electron systems considering the same value of  $\gamma$ .

An optimal tuning procedure was performed for all the long-range corrected hybrid functional tested in this work with the aim of finding the optimal value of the range-separation parameter  $\gamma$  (Figure S1).

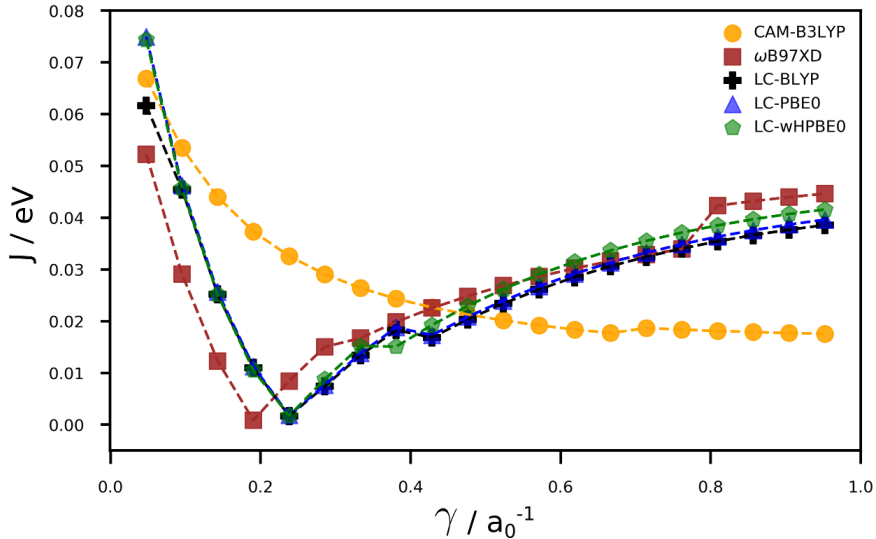


Figure S1: Optimal tuning (Eq. [S1]) of several long-range corrected hybrid functionals for carbazole molecule in vacuum as a function of the range-separation parameter  $\gamma$ . The basis set 6-311++G(d,p) was used in all the cases.

We address the performance of different functionals for the description of the experimental absorption and emission energies (Figure S2). For the long-range corrected functionals, we

consider the values calculated at the optimal value of  $\gamma$  after minimising  $J^2(\gamma)$  (Eq. [S1]), except for  $\omega$ B97XD and CAM-B3LYP functionals where the values defined in Gaussian were used.<sup>S5</sup>

Figure S2 shows the errors for the four lowest electronic transitions energies with respect to the corresponding experimental values in the gas phase.<sup>S6–S8</sup> The errors of different excited states are not uniform and some excitations are described more accurately than others (Fig. S2a). For example, the fluorescence energy obtained with ADC(2)/TZVP is in a very good agreement with the experimental value, however the errors for the vertical excitations  $S_0$ - $S_1$  and  $S_0$ - $S_2$  are in the range 5-10% and for phosphorescence around 20%. Contrary to expected, the cumulative errors for global hybrids PBE0 and B3LYP are smaller than the obtained with long-range corrected functionals and ADC(2).

Considering the good performance of TD-B3LYP/6-311++G(d,p) for the description of the low energy excited states of Cz (up to the second bright state), we have chosen this method for our study. Recent works with focus on Cz and its oligomers have also successfully employed TD-B3LYP.<sup>S9–S12</sup> Table S1 shows the main features of the electronic transitions at the TD-B3LYP/6-311++G(d,p) level of theory.

The predicted structures for  $S_0$ ,  $S_1$ ,  $S_2$  and  $T_1$  states are planar. In line with previous computational and experimental studies, all the transitions show a  $\pi$ - $\pi^*$  character.<sup>S6,S13,S14</sup> The  $S_0 \rightarrow S_1$  and  $S_0 \rightarrow S_2$  excitations have dominant contributions from the HOMO  $\rightarrow$  LUMO and (HOMO-1)  $\rightarrow$  LUMO transitions, as also predicted by SS-CASPT2/cc-pVDZ level of theory.<sup>S15</sup> Both the energies and oscillator strengths of these transitions are in fairly well agreement with the experimental values.<sup>S6,S7</sup> The spin-forbidden transitions  $S_0 \rightarrow T_1$  and  $T_1 \rightarrow S_0$  are dominated by the (HOMO-1)  $\rightarrow$  LUMO and (HOMO)  $\rightarrow$  LUMO, respectively.

Because the symmetry of  $S_1$  state is  $A_1$ , the transition dipole moment of the  $S_0 \rightarrow S_1$  excitation only has a component on the short axis of the molecule ( $C_2$ ).<sup>S13</sup> This excitation has a significant charge transfer character, with a decrease of the electron density on the N atom (see Figure S3). TD-B3LYP predicts an increase of the dipole moment of 0.73 Debye

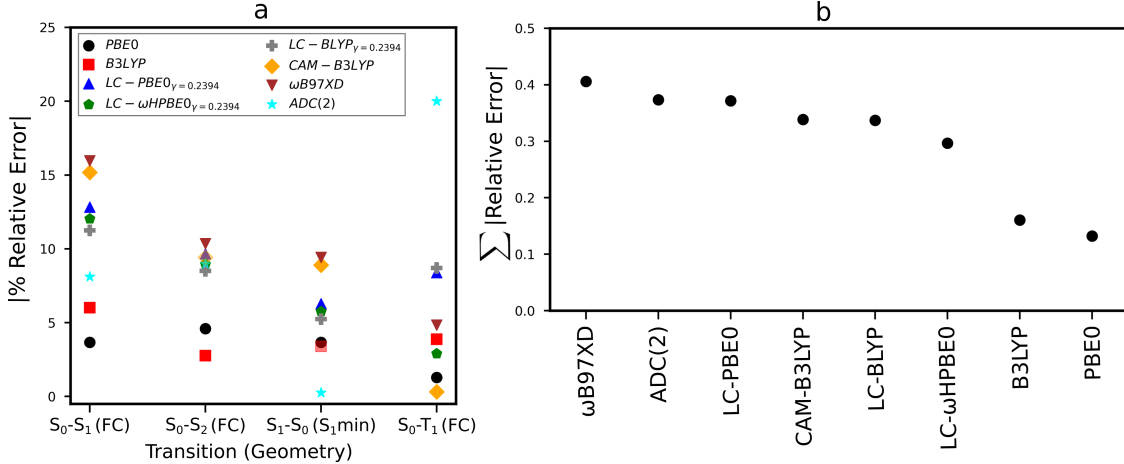


Figure S2: (a) Percentual relative error (in absolute value) for the transitions  $S_0 \rightarrow T_1$ ,  $S_0 \rightarrow S_1$ ,  $S_0 \rightarrow S_2$  and  $S_1 \rightarrow S_0$ . The energies of the first three transitions were calculated at the  $S_0$  equilibrium geometry (FC), whereas the energy of  $S_1 \rightarrow S_0$  was obtained at the  $S_1$  equilibrium geometry ( $S_1$  min). (b) Cumulative percentual error (in absolute value) for the four transitions considered.

for Cz which is in good agreement with the experimental value of 1.1 Debye.<sup>S13</sup>

Table S1: Excitation energies, oscillator strengths ( $f$ ) and orbital contribution for the selected transitions of Cz in the gas phase. The values in brackets correspond to the adiabatic electronic transitions. The orbitals with the highest contribution for each transition are shown in Fig. S2.

Transition	Transition nature	Orbital contribution	TD-B3LYP/6-311++G(d,p)		Experiment	
			Energy / eV	$f$	energy / eV	$f$
$S_0 \rightarrow T_1$	$\pi-\pi^*$	H-1 $\rightarrow$ L (75%)	3.22(2.67)		$3.10^{S6}$	
		H $\rightarrow$ L+2 (12%)				
$S_0 \rightarrow S_1$	$\pi-\pi^*$	H $\rightarrow$ L (92%)	4.05(3.77)	0.030	$3.82^{S7}$	$0.042^{S7}$
		H-1 $\rightarrow$ L (78%)				
$S_0 \rightarrow S_2$	$\pi-\pi^*$	H $\rightarrow$ L+2 (18%)	4.46(4.18)	0.14	$4.35^{S7}$	$0.15^{S7}$
$T_1 \rightarrow S_0$	$\pi-\pi^*$	H $\rightarrow$ L (93%)	2.51(2.65)	$1.5 \cdot 10^{-10}$		
$S_1 \rightarrow S_0$	$\pi-\pi^*$	H $\rightarrow$ L (93%)	3.79(3.77)	0.034	$3.82^{S7}$	

### S1.1 Orbitals and electronic density differences for the monomer in the gas phase

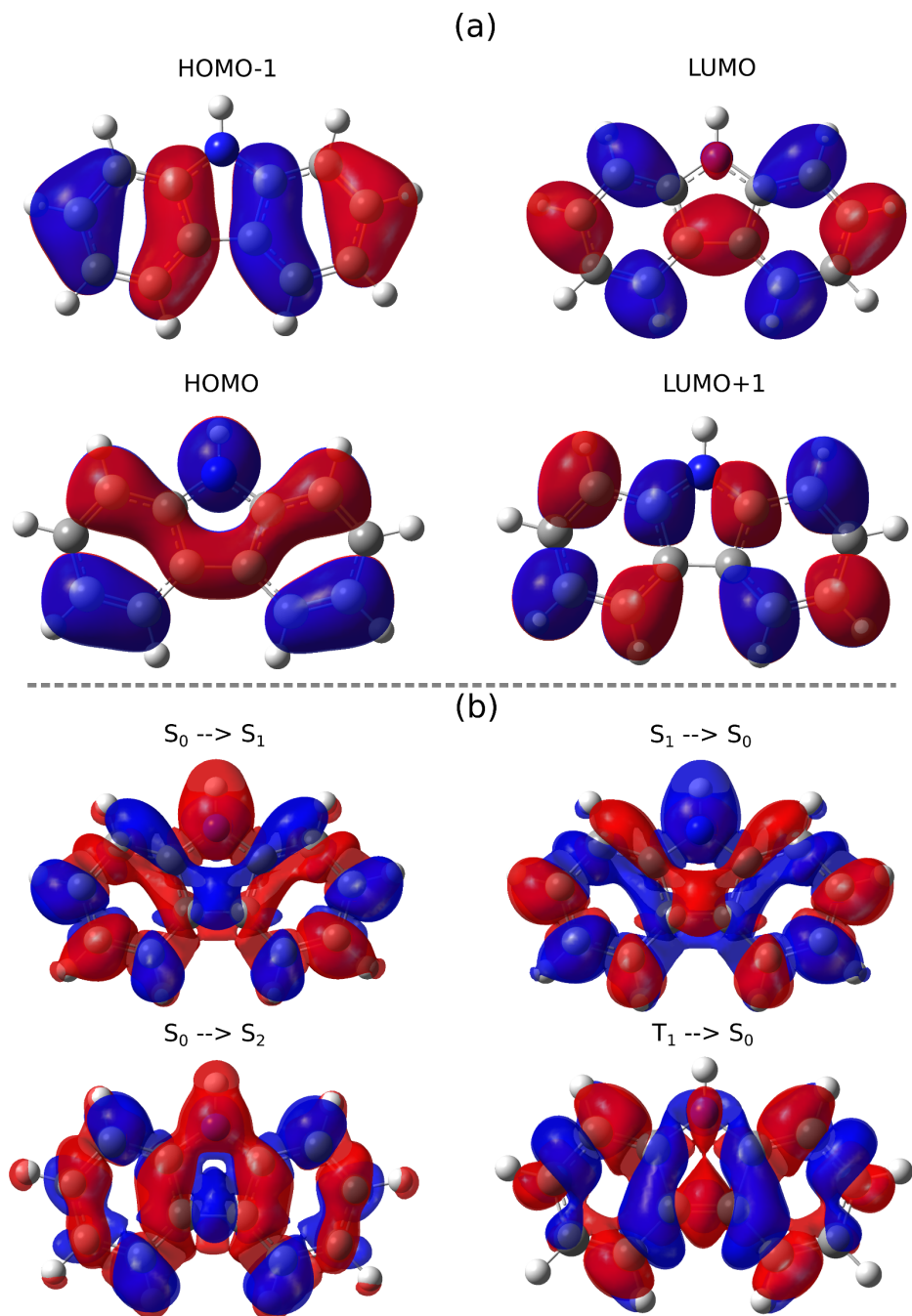


Figure S3: (a) Orbitals involved in the electronic transitions for the  $S_{0\min}$  structure. (b) Density differences (blue positive, red negative) for the four excited states. All the results are obtained with TD-B3LYP/6-311++G(d,p) for carbazole in the gas phase.

## S2 Marcus-Levich-Jortner rate for electron transfer processes

The electronic transfer (ET) rate coefficients for processes such as intersystem crossing, exciton transfer or charge transfer can be obtained by using the Marcus-Levich-Jortner rate equation for electron transfer processes as described in references S16 and S17:

$$k_{ET} = \frac{2\pi}{\hbar} |H_{ab}|^2 F_k, \quad (\text{S2})$$

where  $H_{ab}$  is the electronic coupling operator between the states involved in the ET process.  $F_k$  is the final vibrational state density at the point of the initial state energy level weighted by Franck-Condon (FC) factors  $\sum_l |\langle \theta_{ik} | \theta_{fl} \rangle|^2$ , where  $\theta$  represents the vibrational wavefunctions for both electronic states involved in the electron transfer process. The FC-weighted density of states can be estimated by the Marcus semiclassical approach in the room temperature regime:

$$F_k = \sqrt{\frac{1}{4\pi\lambda_c k_B T}} \sum_n \exp(-s_k) \frac{s_k^n}{n!} \exp\left[-\frac{(\Delta G^\circ + n\hbar\omega_k + \lambda_c)^2}{4\lambda_c k_B T}\right]. \quad (\text{S3})$$

Here,  $\omega_k$  is the frequency of an effective normal mode involved in the exciton transport process. Most intramolecular vibration frequencies are high above the thermal energy at room temperature ( $\approx 210 \text{ cm}^{-1}$ ). Hence, the quantum mechanical vibrational levels must be taken into account for these vibrations. The high-frequency vibrational modes (the quantum modes) "j" are populated only in their ground states and the Franck-Condon factor simplifies to a Poisson distribution ( $|\langle \theta_0 | \theta_k \rangle|^2 = \frac{s_k^n}{n!} e^{-s_k}$ ) in Eq. [S3]. Thus, the most active normal modes  $q_j$  with  $\lambda_j$  are considerably high in the ET process can be merged to one effective vibrational mode with an effective frequency  $\omega_k$ :

$$\omega_k = \frac{\sum_j \omega_j s_j}{\sum_j s_j}, \quad (\text{S4})$$

and an effective dimensionless Huang-Rhys factor

$$s_k = \frac{\sum_j \lambda_j}{\hbar \omega_k} = \omega_k \Delta q_k^2 / 2\hbar, \quad (\text{S5})$$

which describes the relative displacement along the effective quantum normal mode  $q_k$  with energy  $\hbar \omega_k$ .  $\lambda_c$  in Eq. [S3] is the Marcus (or classical) reorganization energy which accounts for low-frequency vibrational modes and those high-frequency modes which do not have an active role in the exciton hopping process.

For an ET process, the intramolecular reorganisation energy  $\lambda$  is related to the geometry relaxation energies of one molecule going from the fully relaxed ground state  $S_0$  to the electronic excited state  $S_n$  or  $T_n$  and a neighboring molecule evolving in the opposite way:

$$\lambda = \lambda_{S(T)_n}^{M_1} + \lambda_{S_0}^{M_2}. \quad (\text{S6})$$

If the ET process is an electron transfer (charge transfer), the reorganization energy of Eq. S6 is obtained by replacing  $\lambda_{S(T)_n}^{M_1}$  by the reorganization energy in the anionic potential energy surface ( $\lambda_{-}^{M_1}$ ). Besides, when the ET process occurs within a homodimer (i. e., the donor and the acceptor are chemically identical), and neglecting any energy difference caused by the environment of each monomer,  $\Delta G^\circ \approx 0$  in Eq. [S3] and the total reorganization energy can be approximated as

$$\lambda \approx 2\lambda_{S_0}^{M_2}. \quad (\text{S7})$$

The reorganization energy of Eq. [S7] can also be obtained within the displaced harmonic oscillator model by the summation of the reorganisation energies projected over the vibrational normal modes  $\lambda_i$  of the  $S_0$  electronic state. This is performed by computing

the Duschinsky rotation matrix, as implemented in the Dushin program.<sup>S18</sup> Rotational and traslational degrees of freedom are excluded from the  $\lambda$  computation due to the fact that the vibrational analysis carried out within the employed cluster models is *de facto* in vacuum with added Coulomb corrections from the electrostatic embedding of the QM/QM'. The classical reorganization energy of Eq. [S3]  $\lambda_c$  is then obtained by subtracting the reorganization energy of the quantum modes "j", i.e. the quantum reorganization energy  $\lambda_k$  to  $\lambda$  as

$$\lambda_c = \lambda - \lambda_k. \quad (\text{S8})$$

### S3 Comparison between embedded cluster models

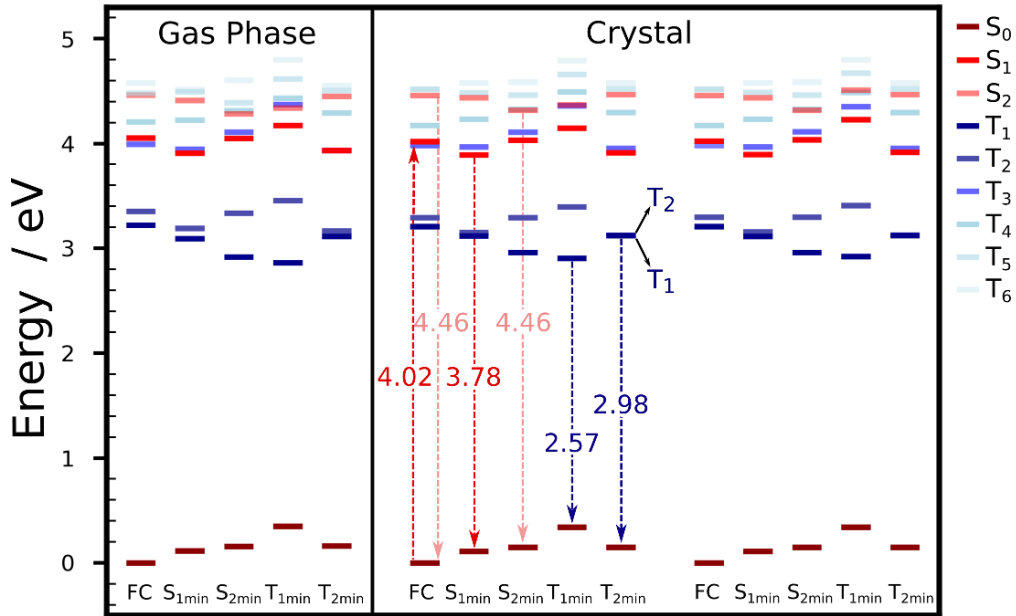


Figure S4: TD-B3LYP/6-311++G(d,p) energies of  $S_0$ - $S_2$  and  $T_1$ - $T_6$  states computed at the critical points in gas phase and in the crystal using the OEC and OEEC models as explained in Section 2 of the manuscript. The results obtained with the OEC and OEEC models are presented in the left and right part of the crystal panel, respectively. The arrows indicate the energies (in eV) for the corresponding vertical transitions computed with the OEC model.

Table S2: Energies (in eV) of the considered electronic states in gas phase and in the crystal within the OEC and OEEC models. All the values are relative to  $S_{0min}$ .

	$S_0$	$S_1$	$S_2$	$T_1$	$T_2$	$T_3$	$T_4$	$T_5$	$T_6$
$S_{0min}$									
Gas Phase	0.000	4.054	4.464	3.223	3.354	3.993	4.208	4.480	4.577
OEC	0.000	4.019	4.458	3.209	3.295	3.980	4.172	4.518	4.520
OEEC	0.000	4.022	4.459	3.208	3.297	3.981	4.173	4.519	4.520
$S_{1min}$									
Gas Phase	0.114	3.907	4.412	3.095	3.192	3.947	4.223	4.495	4.514
OEC	0.111	3.893	4.438	3.118	3.154	3.968	4.232	4.487	4.578
OEEC	0.111	3.896	4.439	3.117	3.156	3.968	4.232	4.488	4.577
$S_{2min}$									
Gas Phase	0.158	4.049	4.283	2.920	3.338	4.111	4.313	4.389	4.602
OEC	0.148	4.033	4.317	2.962	3.294	4.110	4.325	4.465	4.586
OEEC	0.148	4.036	4.318	2.960	3.297	4.111	4.326	4.465	4.587
$T_{1min}$									
Gas Phase	0.351	4.171	4.338	2.861	3.455	4.374	4.435	4.618	4.802
OEC	0.339	4.417	4.371	2.905	3.398	4.360	4.493	4.661	4.793
OEEC	0.339	4.227	4.509	2.921	3.409	4.354	4.491	4.672	4.801
$T_{2min}$									
Gas Phase	0.161	3.934	4.449	3.117	3.168	3.934	4.294	4.507	4.554
OEC	0.149	3.915	4.466	3.124	3.124	3.954	4.296	4.521	4.579
OEEC	0.149	3.918	4.468	3.123	3.126	3.954	4.296	4.523	4.579

## S4 Calculation of fluorescence time constant and quantum yields

We considered the main processes depleting the population of  $S_1$  for the calculation of the fluorescence time constant ( $\tau_f$ ) and quantum yield ( $\Phi_f$ ). We used the the following equations:

$$\tau_f = \frac{1}{k_f + k_{IC} + k_{ISC}} \quad (S9)$$

$$\Phi_f = \frac{k_f}{k_f + k_{IC} + k_{ISC}} = k_f \tau_f \quad (S10)$$

where  $k_f$  is the fluorescence rate coefficient,  $k_{IC}$  stands for the internal conversion rate coefficient from the excited singlet state  $S_n$  to the ground state  $S_0$ ,  $k_{ISC}$  is the global intersystem crossing rate coefficient from  $S_n$  to all the possible triplet states involved.  $k_f$  was calculated using Eq. 1 in the main text. Based on the experimental observations in gas phase and solution, the internal conversion from  $S_1$  to  $S_0$  was neglected ( $k_{IC} = 0$ ).<sup>S13,S19</sup>  $k_{ISC}$  included the contributions from the transitions from  $S_1$  to  $T_4$ ,  $T_3$ ,  $T_2$  and  $T_1$ . Provided the values of the spin orbit couplings and the energy gaps, the transition  $S_1 \rightarrow T_3$  accounted for the 99.9% of the total value.

The phosphorescence time constant ( $\tau_p$ ) was obtained with:

$$\tau_p = \frac{1}{k_p + k'_{ISC} + k'_{IC}} \quad (\text{S11})$$

where  $k_p$  is the phosphorescence rate coefficient,  $k'_{IC}$  is the internal conversion rate coefficient from the excited triplet state  $T_m$  to another excited triplet state of lower energy  $T_l$ ,  $k'_{ISC}$  is the intersystem crossing rate coefficient for  $T_m \rightarrow S_0$ . We assumed  $k'_{IC}=0$  because  $\tau_p$  was computed from the  $T_1$  state.

## S5 The centred molecule mechanism of pure Cz crystal

### S5.1 Spectroscopic characterization

Table S3: Vertical energies and oscillator strengths ( $f$ ) for the selected transitions of Cz crystal considering a monomer in the high-level region (TD-B3LYP/6-311++G(d,p)). The values in brackets correspond to the adiabatic electronic transitions.

Transition	Transition nature	TD-B3LYP/6-311++G(d,p) Energy / eV	$f$	Experiment energy / eV	$f$
$S_0 \rightarrow T_1$	$\pi-\pi^*$	3.21(2.70)	-	-	-
$S_0 \rightarrow S_1$	$\pi-\pi^*$	4.02(3.75)	0.032	3.62 <sup>S10,S20</sup>	0.09 <sup>S20</sup>
$S_0 \rightarrow S_2$	$\pi-\pi^*$	4.46(4.21)	0.12	4.21 <sup>S20</sup>	
$T_1 \rightarrow S_0$	$\pi-\pi^*$	2.57(2.70)		2.25 <sup>S11,S21</sup>	
$T_2 \rightarrow S_0$	$\pi-\pi^*$	2.98(3.10)		2.95 <sup>S10</sup>	
$S_1 \rightarrow S_0$	$\pi-\pi^*$	3.78(3.75)	0.036	3.42 <sup>S21</sup>	

## S5.2 ISC mechanism from $S_2$

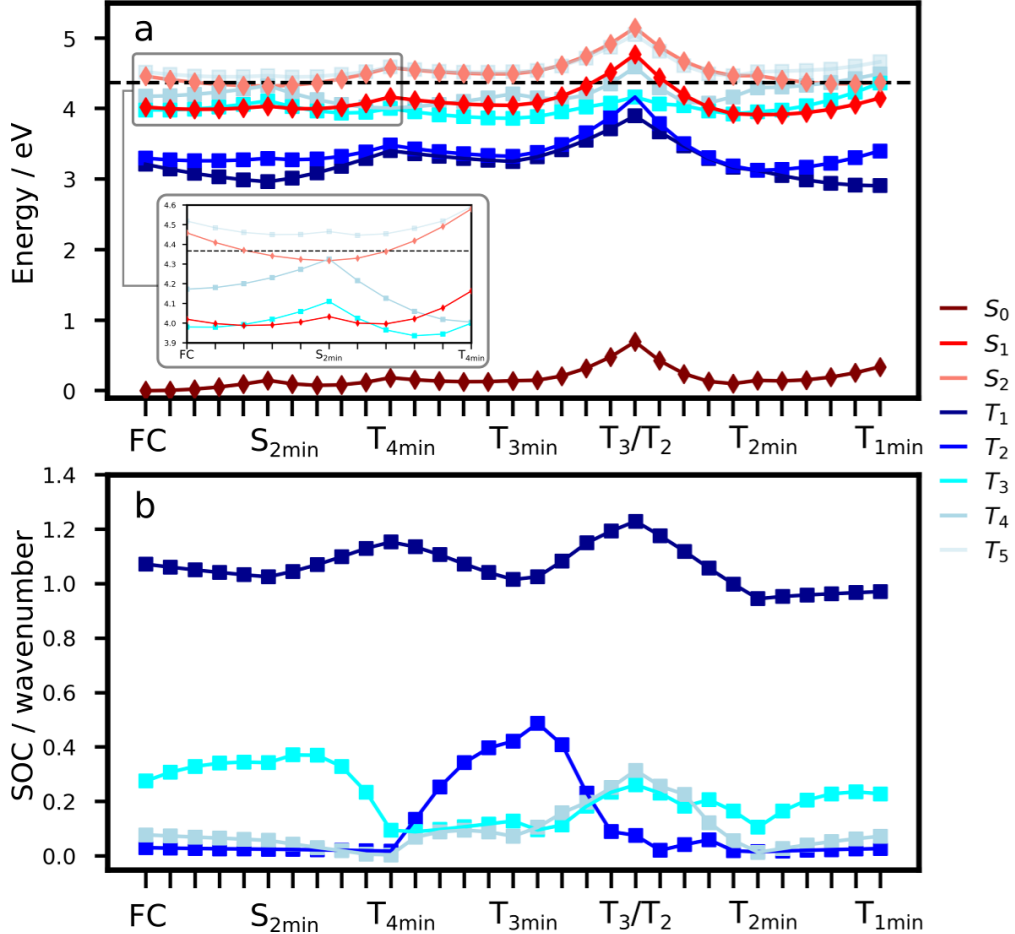


Figure S5: Excitation energies for a centred molecule in the crystal environment (OEC model). (a) TD-B3LYP/6-311++G(d,p) energies along the linear interpolated Cartesian coordinates pathway (LICC) from the FC geometry, after electronic excitation to  $S_2$ , to the minima of the electronic states involved in the mechanism of ISC and phosphorescence processes. The dashed line represents the energy for the  $S_2/S_1$  crossing computed at 4.37 eV. The inset shows a zoomed view of the region of the PES where the internal conversion  $S_2 \rightarrow S_1$  or the intersystem crossing  $S_2 \rightarrow T_4$  may occur. (b) Spin-orbit couplings values along the LICC between  $S_2$  and the first four triplet states. The values are obtained with TD-B3LYP/6-311++G(d,p) as explained in Section 2 of the manuscript.

### S5.3 S<sub>2</sub>/S<sub>1</sub> and T<sub>3</sub>/T<sub>2</sub> crossing geometries

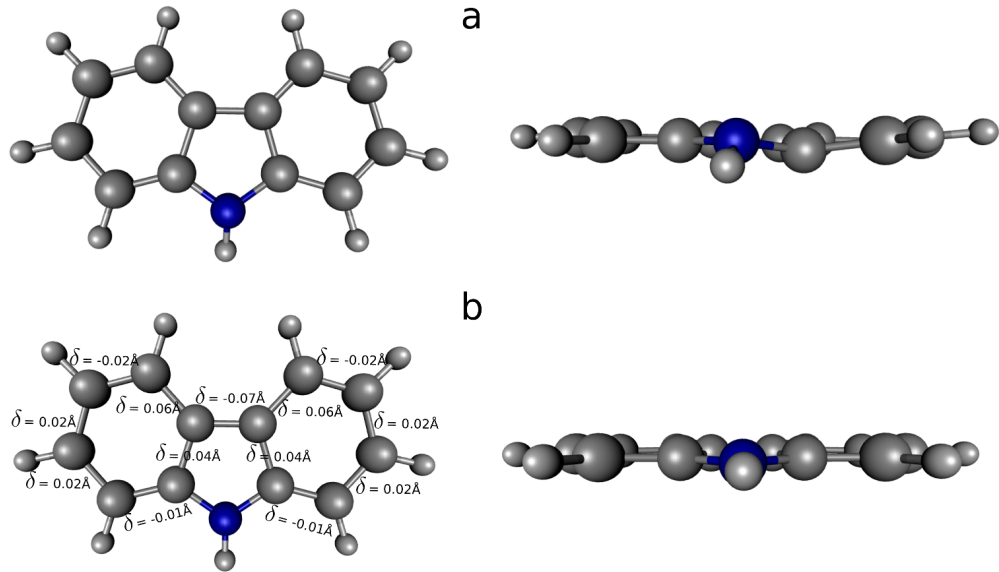


Figure S6: Optimised structures at the T<sub>3</sub>/T<sub>2</sub> (a) and S<sub>2</sub>/S<sub>1</sub> (b) crossings for carbazole crystal using the penalty function method implemented by Levine *et. al.*<sup>S22</sup> at the TD-B3LYP/6-311++G(d,p) level of theory. The main structural differences between the geometries at S<sub>2</sub>/S<sub>1</sub> crossing and at S<sub>0min</sub> (Franck-Condon geometry) are also shown in panel b.

	S <sub>2</sub> /S <sub>1</sub> crossing			T <sub>3</sub> /T <sub>2</sub> crossing			
C	-0.38865	-1.12872	-0.89764	C	-0.50992	-1.1101	-0.73722
C	-0.5596	-2.47033	-1.18636	C	-0.5565	-2.48773	-1.12777
C	0.20527	-0.6911	0.36115	C	0.17439	-0.70491	0.46575
N	-0.70929	0.	-1.62847	N	-0.67453	0.04246	-1.56863
C	-0.09285	-3.38941	-0.21518	C	-0.08038	-3.42574	-0.24252
H	-1.01872	-2.80588	-2.10688	H	-0.98727	-2.7784	-2.07893
C	0.65701	-1.67072	1.33838	C	0.66263	-1.6299	1.32928
C	0.20527	0.6911	0.36114	C	0.22241	0.75748	0.43357
H	-1.13368	0.	-2.54151	H	-1.29692	0.05846	-2.36364
C	-0.38865	1.12872	-0.89764	C	-0.37773	1.18259	-0.83925
C	0.50838	-2.99518	1.01516	C	0.48892	-3.05347	1.01657
H	-0.19494	-4.45003	-0.42093	H	-0.1419	-4.47735	-0.49882
H	1.11079	-1.34597	2.26503	H	1.1779	-1.34269	2.23778
C	0.65701	1.67072	1.33839	C	0.67389	1.72885	1.33077
C	-0.5596	2.47033	-1.18636	C	-0.54601	2.51587	-1.1498
H	0.85798	-3.76308	1.69536	H	0.90172	-3.79836	1.68315
C	0.50838	2.99517	1.01516	C	0.53095	3.05172	1.00387
H	1.11079	1.34597	2.26503	H	1.13112	1.4421	2.27032
C	-0.09285	3.38941	-0.21518	C	-0.09591	3.46089	-0.23593
H	-1.01873	2.80588	-2.10688	H	-1.01369	2.81393	-2.08099
H	0.85798	3.76307	1.69537	H	0.89803	3.8107	1.68584
H	-0.19494	4.45003	-0.42093	H	-0.21067	4.51725	-0.44159

## S5.4 Spin-Orbit coupling values for an embedded molecule

Table S4: Spin-Orbit coupling values (in  $\text{cm}^{-1}$ ) obtained at the  $S_{1min}$  and  $S_{2min}$  geometries within the OEC model with a monomer as the QM region. The PySOC program at the TD-B3LYP/6-311++G(d,p) level of theory was used.

Geometry	T <sub>1</sub>	T <sub>2</sub>	T <sub>3</sub>	T <sub>4</sub>	T <sub>5</sub>
$S_{1min}$	0.984	0.027	0.217	0.058	0.702
$S_{2min}$	0.009	0.938	0.018	0.399	0.831

## S6 Huang-Rhys factors

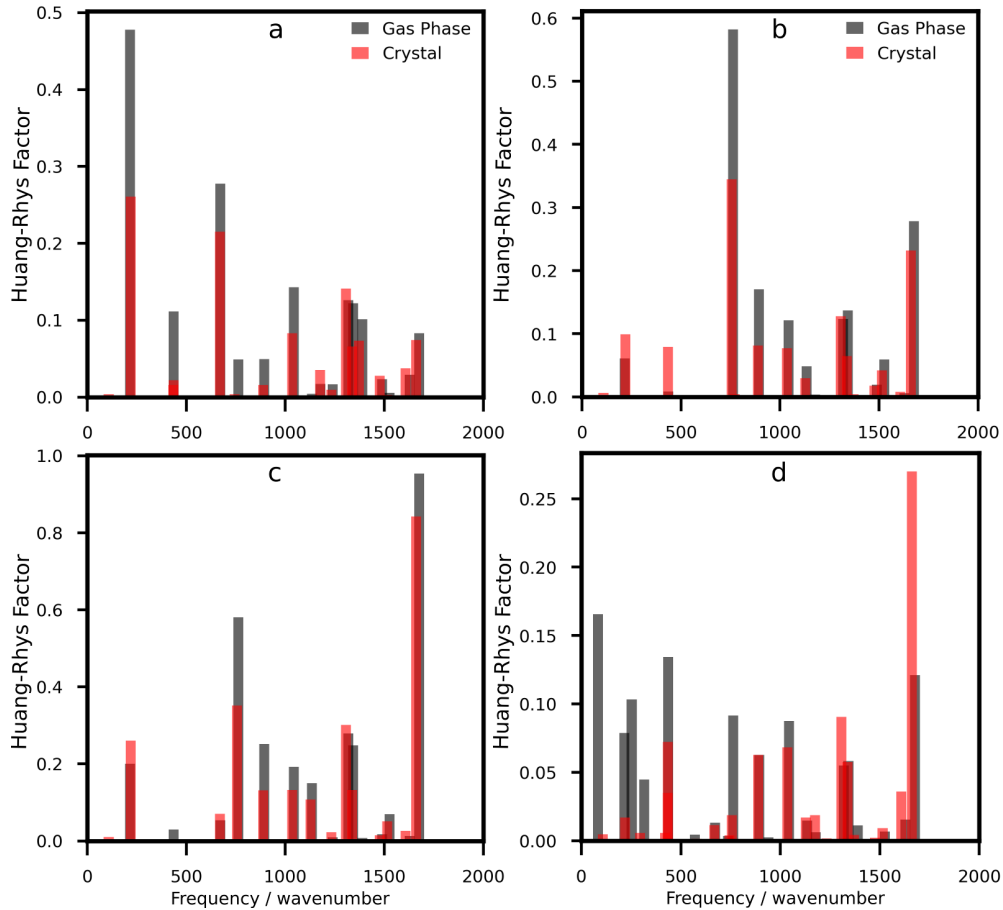


Figure S7: Huang-Rhys factors computed for the  $S_0 \rightarrow S_1$  (a) and  $S_0 \rightarrow S_2$  (b),  $S_0 \rightarrow T_1$  (c),  $S_0 \rightarrow \text{Cz}^-$  (d) transitions of carbazole in gas phase (grey) and in the crystal (red). The Huang-Rhys factors are obtained by computing the Duschinsky rotation matrix, as implemented in the Dushin program,<sup>S18</sup> at the TD-B3LYP/6-311++G(d,p) level of theory.

## S7 Carbazole Dimers

### S7.1 Dimer Structures

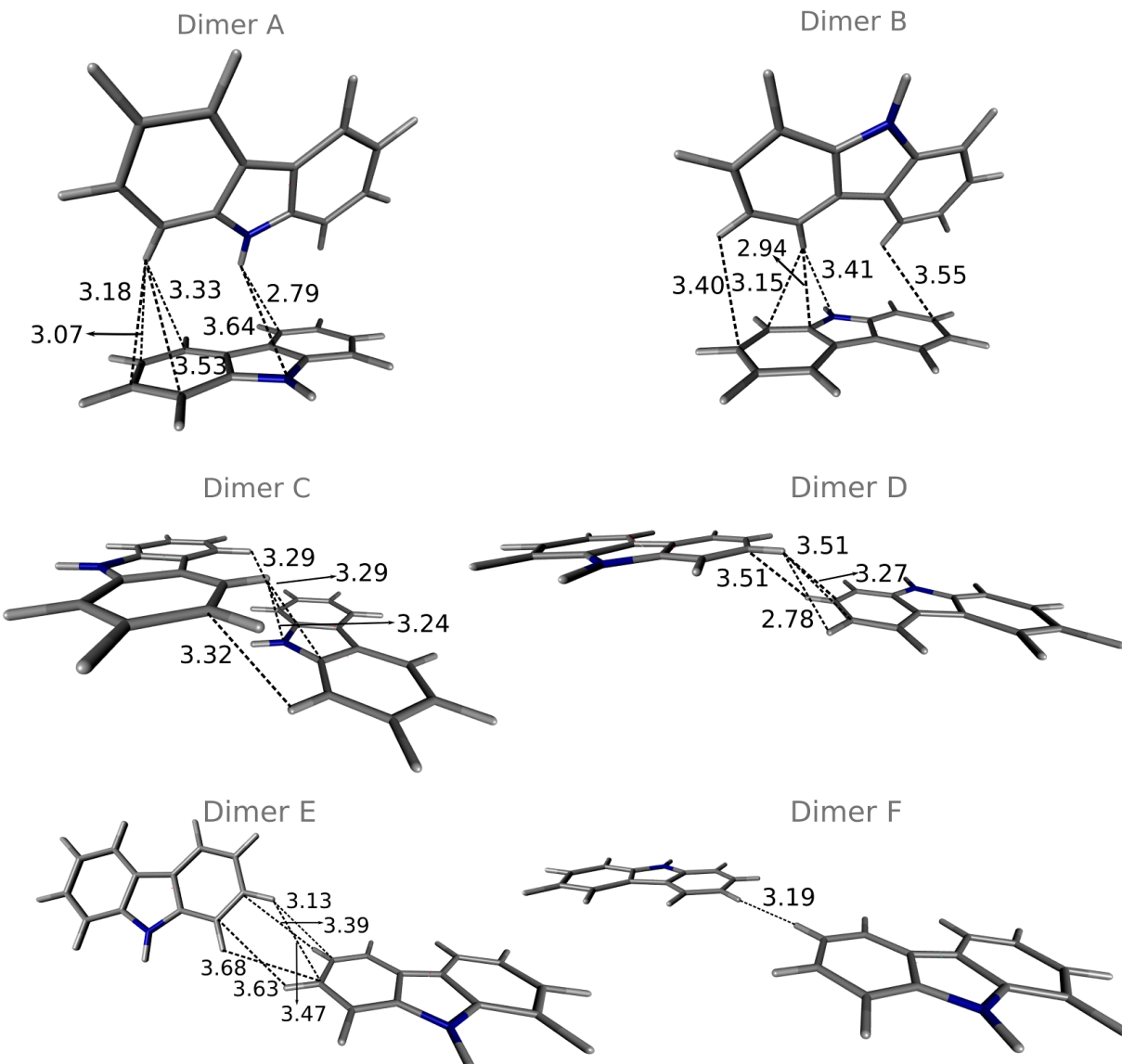


Figure S8: Molecular dimers present in the crystal packing optimised at the TD-B3LYP/6-311++G(d,p) level within the ONIOM Embedded Cluster model. The black dashed lines show the distances (in Å) of the closest atoms within each dimer.

## S7.2 Transition Densities

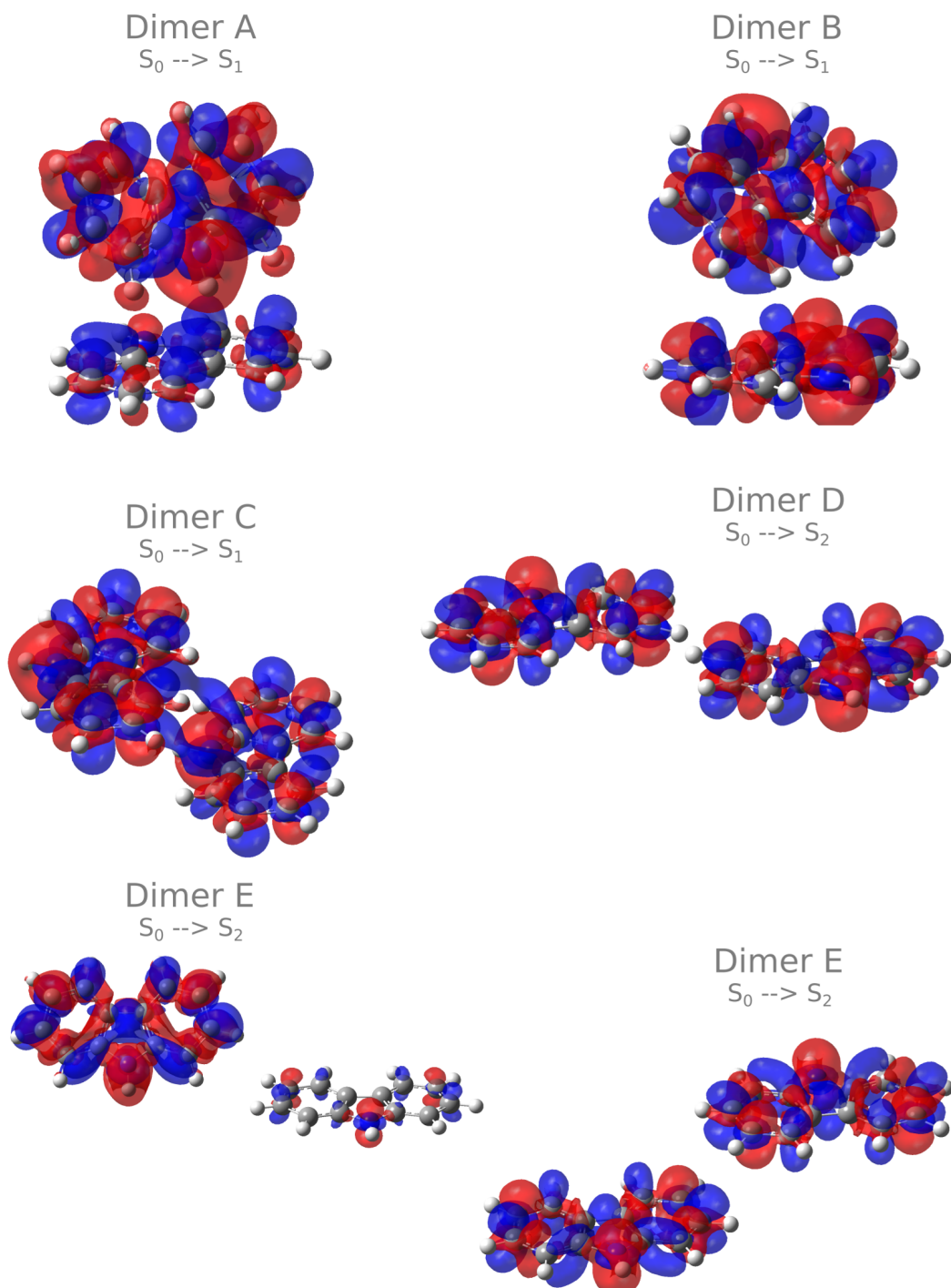


Figure S9: Transition densities (blue positive, red negative) between the ground and the first bright state of each dimer obtained at TD-B3LYP/6-311++G(d,p) level of theory within the OEC model.

### S7.3 Energies and spin-orbit couplings for the embedded dimers

Table S5: Electronic energies (in eV) with respect to  $S_{0min}$  energy computed for each dimer present in the crystal packing using TD-B3LYP/6-311++G(d,p) within the OEC model.

Dimer	Bright State	$S_{Bright}$	T <sub>1</sub>	T <sub>2</sub>	T <sub>3</sub>	T <sub>4</sub>	T <sub>5</sub>	T <sub>6</sub>
A	S <sub>1</sub>	3.89	3.12	3.16	3.32	3.39	3.87	3.96
B	S <sub>1</sub>	3.88	3.11	3.15	3.32	3.40	3.96	4.08
C	S <sub>1</sub>	3.86	3.13	3.15	3.31	3.39	3.95	4.08
D	S <sub>2</sub>	3.96	3.16	3.16	3.23	3.23	3.97	3.97
E	S <sub>2</sub>	3.83	3.16	3.16	3.22	3.22	3.97	3.97
F	S <sub>2</sub>	3.83	3.16	3.16	3.22	3.22	3.97	3.97

Table S6: Spin-orbit couplings (in cm<sup>-1</sup>) considering each dimer present in the crystal packing at the  $S_{1min}$ . The values are obtained using the PySOC program,<sup>S23</sup> with TD-B3LYP/6-311++G(d,p) within the OEC model.

Dimer	Bright State	T <sub>1</sub>	T <sub>2</sub>	T <sub>3</sub>	T <sub>4</sub>	T <sub>5</sub>	T <sub>6</sub>
A	S <sub>1</sub>	1.204	0.006	0.006	0.015	0.356	0.258
B	S <sub>1</sub>	0.616	0.057	0.041	0.095	0.039	0.205
C	S <sub>1</sub>	0.910	0.047	0.098	0.022	0.183	0.016
D	S <sub>2</sub>	1.008	0.012	0.019	0.045	0.248	0.001
E	S <sub>2</sub>	0.760	0.654	0.061	0.027	0.198	0.150
F	S <sub>2</sub>	0.959	0.304	0.005	0.032	0.243	0.027

### S7.4 Phosphorescence from Cz dimers

Table S7: Phosphorescence energies and electric transition dipole moment from T<sub>1</sub> computed for the 6 dimers present in the crystal packing with TD-B3LYP/6-311++G(d,p). The values of the monomer are also included for comparison.

Structure	E <sub>T<sub>1</sub></sub> (eV)	$\tau_p^{T_1}$ (s)	$\mu_{T_1 \rightarrow S_0}$ (Debye)
Monomer	2.57	7.2	$6.21 \cdot 10^{-9}$
Dimer A	2.57	8.1	$5.46 \cdot 10^{-9}$
Dimer B	2.56	4.6	$9.68 \cdot 10^{-9}$
Dimer C	2.57	7.7	$5.74 \cdot 10^{-9}$
Dimer D	2.56	7.2	$6.20 \cdot 10^{-9}$
Dimer E	2.57	7.4	$6.08 \cdot 10^{-9}$
Dimer F	2.56	7.2	$6.15 \cdot 10^{-9}$

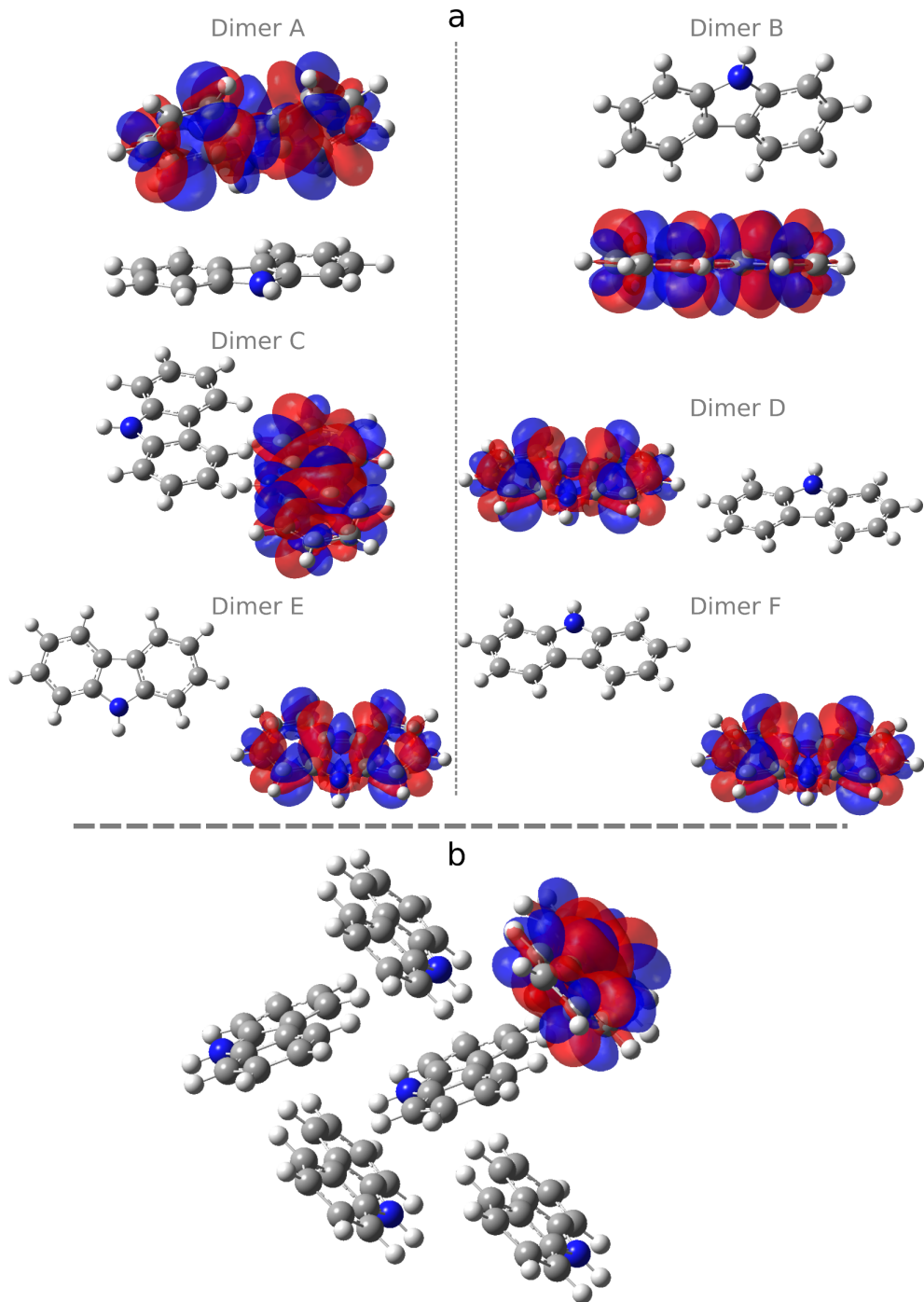


Figure S10:  $T_1 \rightarrow S_0$  density differences computed for the six dimers present in the crystal packing (a) and for a six molecules cluster (all of them treated quantum mechanically) (b) with TD-B3LYP/6-311++G(d,p).

Table S8: Excitation energies from  $S_0$  and oscillator strengths ( $f$ ) computed for a Cz cluster containing six molecules at the TD-B3LYP/6-311++G(d,p) level of theory.

$S_0 \rightarrow$	T <sub>1</sub>	T <sub>2</sub>	T <sub>3</sub>	T <sub>4</sub>	T <sub>5</sub>	T <sub>6</sub>	S <sub>1</sub>	S <sub>2</sub>	S <sub>3</sub>	S <sub>4</sub>	S <sub>5</sub>	S <sub>6</sub>	S <sub>7</sub>	S <sub>8</sub>	S <sub>9</sub>
Energy	3.13	3.14	3.15	3.15	3.16	3.17	3.73	3.80	3.82	3.86	3.88	3.89	3.93	3.95	3.97
$f$							0.011	0.008	0.004	0.016	0.022	0.008	0.042	0.032	0.011

## S7.5 Exciton transport in the triplet manifold

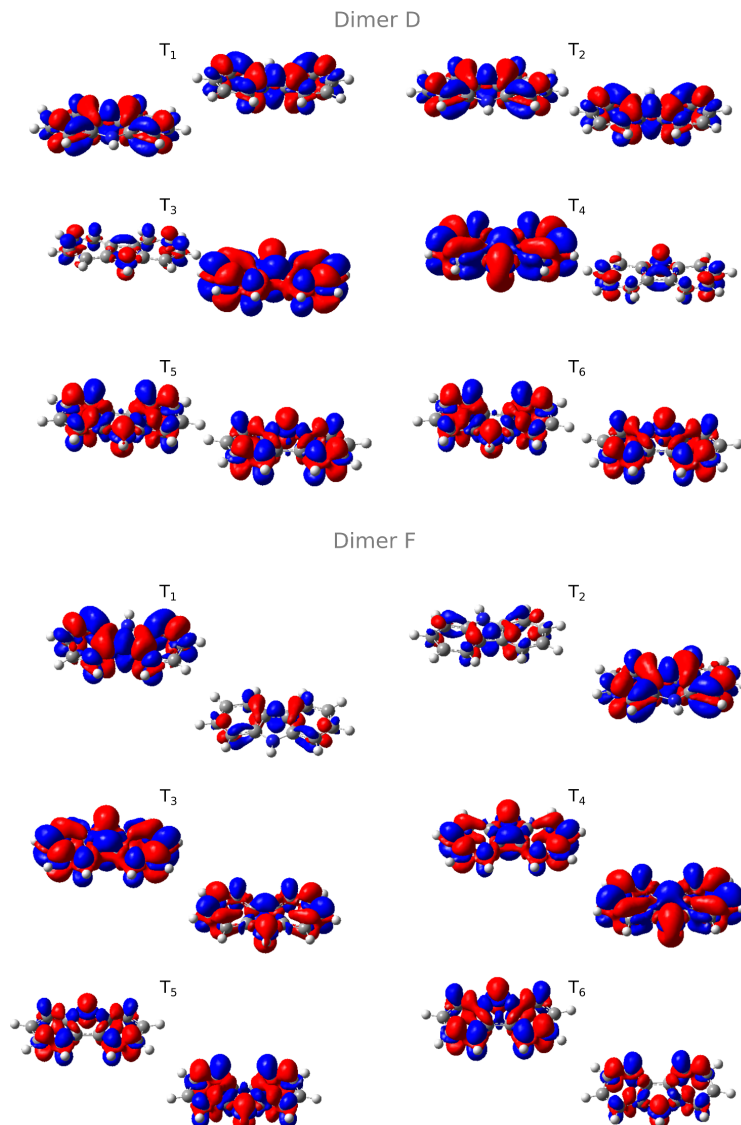


Figure S11:  $T_n \rightarrow S_0$  density differences computed for dimers D and F in the crystal with TD-B3LYP/6-311++G(d,p) within the OEC model.

## S7.6 S<sub>0min</sub> Dimer Coordinates

Dimer A:			Dimer B:			Dimer C:					
N	-1.310085	0.000001	-0.049102	N	-2.675834	-0.000001	-3.072082	N	-0.786011	0.000002	-1.468922
N	2.662594	0.000001	0.101540	C	2.183758	0.725447	1.048187	C	0.689528	1.697574	1.621755
C	-1.638997	1.132366	0.678684	C	-2.350935	-1.132896	-2.344311	C	-0.413802	1.133352	-2.174906
C	-1.638998	-1.132365	0.678682	H	-3.073710	-0.000000	-3.997522	C	-0.413800	-1.133357	-2.174906
H	-0.829425	0.000000	-0.935749	C	-2.350936	1.132894	-2.344309	H	-1.224322	-0.000000	-0.561092
C	2.315758	-1.132870	-0.616400	C	1.588973	1.133092	2.271505	C	0.522566	3.040420	1.937809
C	2.315757	1.132867	-0.616399	C	2.631357	1.695047	0.144567	C	0.230157	0.725817	2.517935
H	3.083241	0.000001	1.017295	C	2.183761	-0.725449	1.048186	H	1.175360	1.412197	0.696544
C	-1.471600	2.481574	0.358158	C	-2.517060	-2.480464	-2.670082	C	-0.591639	2.482864	-1.859742
C	-2.217684	0.725154	1.910521	C	-1.783749	-0.725813	-1.107064	C	0.223622	0.725212	-3.377039
C	-1.471601	-2.481570	0.358158	C	-1.783752	0.725810	-1.107066	C	-0.591639	-2.482864	-1.859741
C	-2.217686	-0.725155	1.910522	C	-2.517061	2.480466	-2.670080	C	0.223624	-0.725214	-3.377041
C	2.491702	-2.481639	-0.298619	C	1.419149	2.481188	2.591798	H	0.890556	3.798252	1.255912
C	1.713582	-0.724935	-1.837081	N	1.240071	0.000000	2.989650	C	-0.106896	3.423598	3.134460
C	2.491702	2.481639	-0.298620	C	2.478400	3.038258	0.464163	C	0.230157	-0.725815	2.517933
C	1.713580	0.724936	-1.837083	H	3.093133	1.405875	-0.792122	C	-0.384908	1.132736	3.732148
C	-1.900110	3.423408	1.288559	C	1.588977	-1.133092	2.271507	C	-0.109306	3.424593	-2.764093
H	-1.019003	2.781265	-0.579590	C	2.631362	-1.695050	0.144568	H	-1.093174	2.783283	-0.947636
C	-2.646356	1.695209	2.822063	C	-2.087142	-3.424454	-1.743170	C	0.697192	1.695182	-4.266094
C	-1.900109	-3.423408	1.288560	H	-2.969582	-2.777588	-3.608826	C	-0.109306	-3.424598	-2.764096
H	-1.019003	-2.781265	-0.579590	C	-1.358486	-1.698363	-0.194628	H	-1.093174	-2.783284	-0.947636
C	-2.646356	-1.695206	2.822065	C	-1.358488	1.698362	-0.194629	C	0.697192	-1.695183	-4.266095
C	2.035502	-3.423948	-1.215143	C	-2.087142	3.424454	-1.743170	C	-0.566013	2.480416	4.048433
H	2.970516	-2.781972	0.626406	H	-2.969581	2.777586	-3.608826	H	-0.231348	4.478038	3.351155
C	1.265627	-1.695577	-2.739548	C	1.871082	3.423007	1.672195	C	0.689527	-1.697576	1.621749
C	2.035502	3.423951	-1.215146	H	0.947483	2.779774	3.520927	C	-0.384907	-1.132738	3.732150
H	2.970517	2.781973	0.626409	H	0.849394	-0.000001	3.918535	N	-0.738132	-0.000003	4.446619
C	1.265626	1.695580	-2.739550	H	2.835951	3.794240	-0.225416	H	-0.229592	4.479651	-2.545493
C	-2.489796	3.038605	2.505361	C	1.419152	-2.481188	2.591798	C	0.534567	3.038749	-3.952527
H	-1.781600	4.478281	1.067830	C	2.478401	-3.038261	0.464165	H	1.187277	1.405799	-5.187828
H	-3.098544	1.405641	3.762982	H	3.093136	-1.405877	-0.792121	H	-0.229592	-4.479653	-2.545492
C	-2.489793	-3.038602	2.505361	C	-1.507058	-3.040730	-0.521889	C	0.534565	-3.038751	-3.952526
H	-1.781601	-4.478279	1.067830	H	-2.196122	-4.479007	-1.969245	H	1.187277	-1.405801	-5.187828
H	-3.098543	-1.405640	3.762981	H	-0.909140	-1.414989	0.749930	H	-1.053008	2.777341	4.969832
C	1.420387	-3.039047	-2.419327	C	-1.507058	3.040730	-0.521890	C	0.522562	-3.040420	1.937809
H	2.155465	-4.478543	-0.993637	H	-0.909139	1.414988	0.749933	H	1.175360	-1.412196	0.696541
H	0.802644	-1.408326	-3.676435	H	-2.196122	4.479005	-1.969246	C	-0.566011	-2.480421	4.048434
C	1.420387	3.039046	-2.419329	H	1.754695	4.477841	1.892569	H	-1.155295	0.000001	5.363839
H	2.155464	4.478545	-0.993636	C	1.871086	-3.423009	1.672193	H	0.915126	3.793209	-4.631411
H	0.802646	1.408328	-3.676432	H	0.947480	-2.779773	3.520927	H	0.915126	-3.793208	-4.631410
H	-2.837166	3.793641	3.201242	H	2.835944	-3.794240	-0.225417	H	0.890558	-3.798252	1.255918
H	-2.837168	-3.793641	3.201242	H	-1.158425	-3.798479	0.169868	C	-0.106898	-3.423601	3.134462
H	1.057288	-3.794080	-3.107283	H	-1.158424	3.798477	0.169868	H	-1.053012	-2.777343	4.969830
H	1.057290	3.794080	-3.107280	H	1.754694	-4.477842	1.892570	H	-0.231347	-4.478043	3.351159

**Dimer D:**

N	-2.005930	-4.863141	-1.516340
N	2.006036	4.863142	1.516287
C	-1.660886	-5.994826	-0.795221
H	-2.417855	-4.864677	-2.435913
C	-1.670492	-3.729036	-0.794726
C	1.670545	3.729036	0.794698
C	1.660937	5.994826	0.795193
H	2.417788	4.864675	2.435937
C	-1.828546	-7.343719	-1.114137
C	-1.070410	-5.585078	0.430071
C	-1.077891	-4.135029	0.431147
C	-1.848284	-2.381226	-1.113915
C	1.848288	2.381226	1.113913
C	1.077912	4.135029	-0.431161
C	1.828550	7.343718	1.114136
C	1.070432	5.585078	-0.430087
C	-1.375104	-8.283490	-0.193694
H	-2.300360	-7.644567	-2.042319
C	-0.619853	-6.552541	1.334259
C	-0.643442	-3.164113	1.339729
C	-1.408791	-1.437968	-0.189972
H	-2.317356	-2.081929	-2.044176
C	1.408800	1.437968	0.189966
H	2.317297	2.081934	2.044206
C	0.643433	3.164112	-1.339728
C	1.375113	8.283491	0.193688
H	2.300299	7.644564	2.042352
C	0.619845	6.552542	-1.334260
C	-0.766882	-7.896106	1.013477
H	-1.489487	-9.338310	-0.414689
H	-0.156713	-6.262309	2.269925
C	-0.805522	-1.821740	1.021060
H	-0.181964	-3.451097	2.277425
H	-1.528035	-0.383833	-0.412520
C	0.805550	1.821738	-1.021075
H	1.528010	0.383834	0.412531
H	0.181873	3.451095	-2.277384
C	0.766911	7.896107	-1.013492
H	1.489467	9.338310	0.414703
H	0.156623	6.262313	-2.269885
H	-0.398999	-8.649723	1.700182
H	-0.453198	-1.065719	1.712753
H	0.453263	1.065716	-1.712785
H	0.399061	8.649724	-1.700214

**Dimer E:**

N	-0.058507	-4.843198	-0.044108
C	-0.863619	4.114008	-1.064359
C	0.280239	-5.981439	0.670069
H	-0.453328	-4.836784	-0.971174
C	0.288483	-3.715954	0.682685
C	-0.277437	3.722352	-2.298000
C	-1.294932	3.132598	-0.165459
C	-0.868485	5.564026	-1.048235
C	0.109170	-7.327288	0.340245
C	0.870303	-5.582734	1.899142
C	0.874336	-4.132632	1.908066
C	0.130010	-2.365291	0.367384
C	-0.105194	2.378557	-2.634881
N	0.058280	4.864067	-3.006991
C	-1.134764	1.793559	-0.499703
H	-1.751773	3.409164	0.777611
C	-0.283267	5.987458	-2.271311
C	1.315776	-6.558502	2.796636
C	-1.310765	6.521788	-0.129965
C	0.558724	-8.275447	1.253913
H	-0.359987	-7.619951	-0.591939
C	1.315776	-6.558502	2.796636
C	1.320893	-3.169641	2.819081
C	0.582430	-1.429865	1.293525
H	-0.330883	-2.059321	-0.564741
C	-0.541400	1.425563	-1.719985
H	0.357240	2.090558	-3.571850
H	0.458345	4.876151	-3.931735
H	-1.478390	1.028027	0.186014
C	-0.115285	7.339648	-2.575330
C	-1.159601	7.868816	-0.433461
H	-1.769836	6.220717	0.804269
C	1.165483	-7.899054	2.465190
H	0.443803	-9.328262	1.023706
H	1.778920	-6.276848	3.734913
C	1.179292	-1.823930	2.503939
H	1.777536	-3.465978	3.756088
H	0.477840	-0.374069	1.072233
H	-0.425115	0.374463	-1.956427
C	-0.559127	8.269304	-1.639865
H	0.351216	7.649120	-3.503330
H	-1.517746	8.615481	0.265889
H	1.530776	-8.659237	3.146056
H	1.544168	-1.074224	3.196611
H	-0.443509	9.326723	-1.846986

**Dimer F:**

N	2.003754	-4.809704	4.373134
N	-2.003771	4.809704	-4.373126
C	1.661347	-5.940657	3.649531
C	1.663253	-3.674658	3.655191
H	2.403272	-4.812385	5.298168
C	-1.663254	3.674658	-3.655192
H	-2.403264	4.812391	-5.298172
C	-1.661340	5.940656	-3.649535
C	1.828426	-7.289984	3.967917
C	1.073615	-5.529462	2.423210
C	1.832249	-2.327176	3.980515
C	1.074793	-4.078938	2.426817
C	-1.832252	2.327176	-3.980515
C	-1.074771	4.078937	-2.426828
C	-1.073593	5.529459	-2.423223
C	-1.828425	7.289982	-3.967919
C	1.378765	-8.229593	3.045232
H	2.295845	-7.591995	4.898063
C	0.629014	-6.497033	1.515906
C	1.383739	-1.382222	3.062822
C	-0.631837	3.106137	-1.524331
C	-0.629003	6.497035	-1.515911
C	-1.378754	8.229592	-3.045239
H	-2.299899	2.030268	-4.912176
C	-0.295865	7.591989	-4.898057
C	0.776277	-7.841112	1.835500
H	1.491774	-9.284801	3.266579
H	0.172282	-6.206360	0.577047
C	0.781117	-1.764034	1.851140
H	1.497103	-0.328165	3.289600
H	0.174397	-3.391253	0.584077
C	-0.781117	1.764032	-1.851141
H	-1.497074	0.328165	-3.289614
H	-0.174393	3.391252	-0.584082
C	-0.776274	7.841112	-1.835505
H	-0.172291	6.206360	-0.577045
H	-1.491759	9.284799	-3.266586
H	0.414074	-8.594361	1.145225
H	0.419089	-1.006667	1.165493
H	-0.419126	1.006664	-1.165479
H	-0.414099	8.594363	-1.145217

## S8 HOMO and LUMO energies

Table S9: HOMO and LUMO energies computed for carbazole crystal (Cz) and the isomer 1H-benzo[f]indole (Bd) embedded in a Cz crystal at the TD-B3LYP/6-311++G(d,p) level of theory. The values measured in a solution of dichloromethane  $5 \times 10^{-4}$  M taken from Ref S21 (shown in brackets) are included for comparison.

System	HOMO (eV)	LUMO eV)
Cz	-5.8 (-5.5) <sup>S21</sup>	-1.2 (-2.0) <sup>S21</sup>
Bd	-5.1 (-5.1) <sup>S21</sup>	-1.2 (-1.8) <sup>S21</sup>

## S9 Bd-Cz dimers

### S9.1 Dimer A

#### S9.1.1 Effect of long-range electrostatic interactions

Table S10: Energies (in eV) of singlet  $\text{Cz}^- \text{Bz}^+$  charge transfer state ( $S_{CT}$ ) with respect to  $S_{0min}$  of dimer A computed with C-DFT at the equilibrium geometries for  $S_0$  ( $S_{0min}$  or FC),  $S_1$  ( $S_{1min}$ ) and  $S_{CT}$  ( $S_{CTmin}$ ) states.

Geometry	OEC	OEEC
FC	4.47	4.43
$S_{1min}$	4.27	4.23
$S_{CTmin}$	3.70	3.69

### S9.1.2 ADC(2) energies of dimer A

Table S11: Electronic energies (in eV) with respect to  $S_{0min}$  (FC) computed for dimer A at the ADC(2)/TZVP level of theory within the OEC model. The point charges were computed with TD-B3LYP/6-311++G(d,p). The main character of the state is included in brackets.

Cz-Cz			
Electronic State	FC	$S_{1min}$	$S_{CTmin}$
$S_0$	0.000 ( $\pi$ )	0.121 ( $\pi$ )	0.4241 ( $\pi$ )
$S_1$	4.053 ( $\pi\pi^*$ )	3.9092 ( $\pi\pi^*$ )	4.1230 ( $\pi\pi^*$ )
$S_2$	4.065 ( $\pi\pi^*$ )	4.170 ( $\pi\pi^*$ )	4.2210 (CT)
$S_3$	4.703 ( $\pi\pi^*$ )	4.698 ( $\pi\pi^*$ )	4.2740 ( $\pi\pi^*$ )
$S_4$	4.742 ( $\pi\pi^*$ )	4.849 ( $\pi\pi^*$ )	4.8159 ( $\pi\pi^*$ )
$S_5$	5.233 ( $\pi\pi^*$ )	5.264 ( $\pi\pi^*$ )	4.9828 (CT)
$S_6$	5.307 ( $\pi\pi^*$ )	5.381 ( $\pi\pi^*$ )	5.0570 ( $\pi\pi^*$ )
Bd-Cz			
Electronic State	FC	$S_{1min}$	$S_{CTmin}$
$S_0$	0.000 ( $\pi$ )	0.057 ( $\pi$ )	0.176 ( $\pi$ )
$S_1$	3.793 ( $\pi\pi^*$ )	3.476 ( $\pi\pi^*$ )	3.562 ( $\pi\pi^*$ )
$S_2$	4.040 ( $\pi\pi^*$ )	4.081 ( $\pi\pi^*$ )	4.007 ( $\pi\pi^*$ )
$S_3$	4.184 ( $\pi\pi^*$ )	4.106 ( $\pi\pi^*$ )	4.050 ( $CT_{Bd \rightarrow Cz}$ )
$S_4$	4.717 ( $\pi\pi^*$ )	4.374 ( $\pi\pi^*$ )	4.145 ( $\pi\pi^*$ )
$S_5$	4.832 ( $CT_{Bd \rightarrow Cz}$ )	4.767 ( $CT_{Bd \rightarrow Cz}$ )	4.691 ( $CT_{Bd \rightarrow Cz}$ )
$S_6$	5.131 ( $CT_{Cz \rightarrow Bd}$ )	4.967 ( $CT_{Bd \rightarrow Cz}$ )	4.785 ( $\pi\pi^*$ )

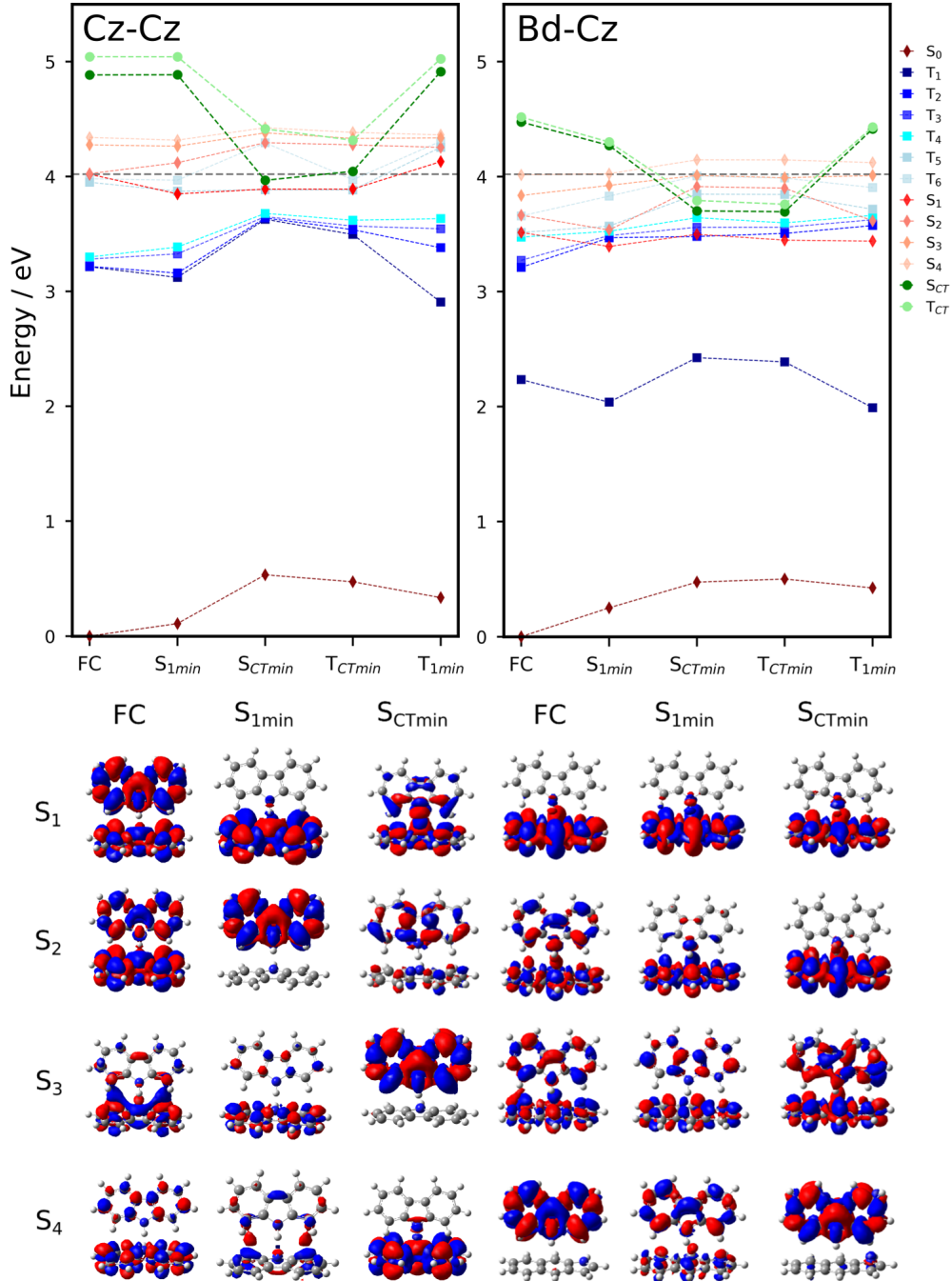


Figure S12: TD-B3LYP/6311++G(d,p) energies of  $S_0$ - $S_4$ ,  $T_1$ - $T_6$ , and singlet and triplet  $Cz^-Cz^+$ ( $Bd^+$ ) charge transfer states ( $S_{CT}$  and  $T_{CT}$ , respectively) computed at the critical points of dimer A in the crystal using the OEC model. The dashed line represents the computed initial excitation energy to the first bright state. The transition densities from  $S_0$  to the  $S_1$ - $S_4$  states for selected geometries are also included.

## S9.2 Dimer B

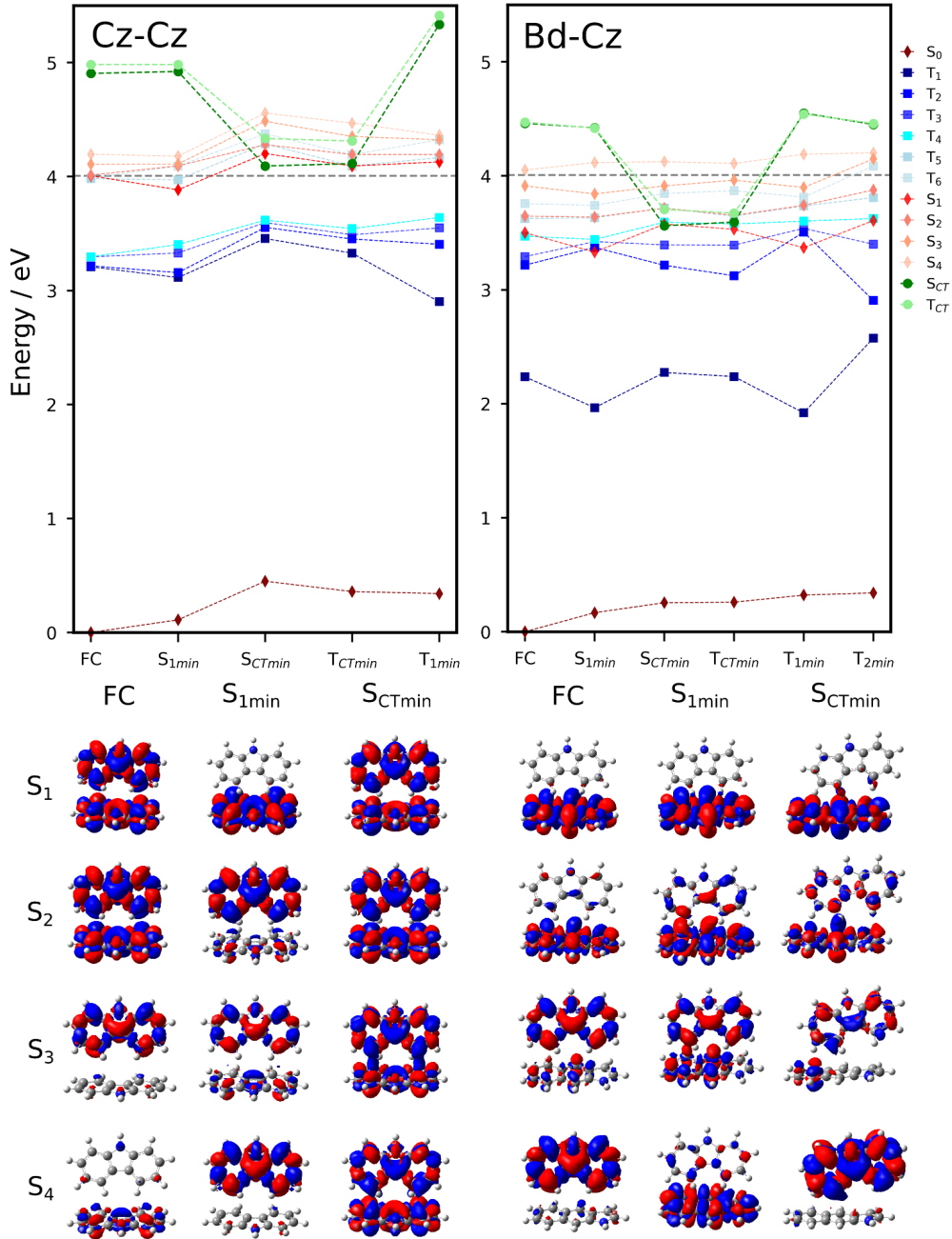


Figure S13: TD-B3LYP/6311++G(d,p) energies of S<sub>0</sub>-S<sub>4</sub>, T<sub>1</sub>-T<sub>6</sub>, and singlet and triplet Cz<sup>-</sup>Cz<sup>+</sup>(Bd<sup>+</sup>) charge transfer states (S<sub>CT</sub> and T<sub>CT</sub>, respectively) computed at the critical points of dimer B in the crystal using the OEC model. The dashed line represents the computed initial excitation energy to the first bright state. The transition densities from S<sub>0</sub> to the S<sub>1</sub>-S<sub>4</sub> states for selected geometries are also included.

### S9.3 Dimer C

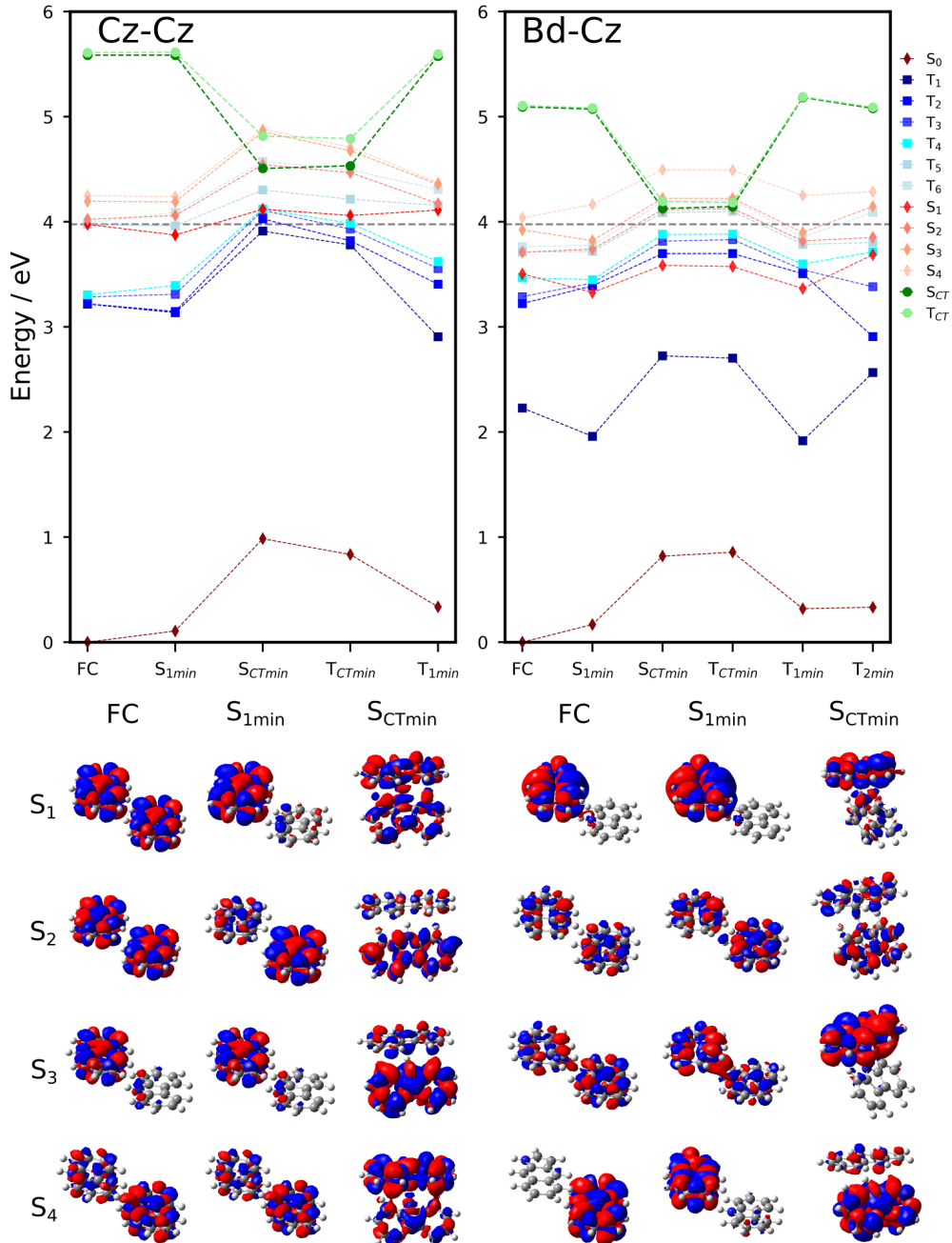


Figure S14: TD-B3LYP/6311++G(d,p) energies of  $S_0$ - $S_4$ ,  $T_1$ - $T_6$ , and singlet and triplet  $\text{Cz}^-$  $\text{Cz}^+$ ( $\text{Bd}^+$ ) charge transfer states ( $S_{CT}$  and  $T_{CT}$ , respectively) computed at the critical points of dimer C in the crystal using the OEC model. The dashed line represents the computed initial excitation energy to the first bright state. The transition densities from  $S_0$  to the  $S_1$ - $S_4$  states for selected geometries are also included.

## S10 Cz<sup>-</sup> absorption transitions

Table S12: Absorption energies (in eV) of a Cz<sup>-</sup> molecule in the crystal computed at TD-B3LYP/6-311++G(d,p) and ADC(2)/TZVP level of theories within the OEC model. The point charges were computed with TD-B3LYP/6-311++G(d,p) in both cases.

Transition nature	TD-B3LYP/6-311++G(d,p)	ADC(2)/TZVP
$\pi\pi^*$	1.23 $f = 0.01$	1.53 $f = 0.04$
$\pi\pi^*$	1.58 $f = 0.003$	1.93 $f = 0.003$
$\pi\pi^*$	2.07 $f = 0.12$	2.28 $f = 0.17$

## References

- (S1) Frisch, M. J.; Trucks, G. W.; Schlegel, H. B.; Scuseria, G. E.; Robb, M. A.; Cheeseman, J. R.; Scalmani, G.; Barone, V.; Petersson, G. A.; Nakatsuji, H.; Li, X.; Caricato, M.; Marenich, A. V.; Bloino, J.; Janesko, B. G.; Gomperts, R.; Mennucci, B.; Hratchian, H. P.; Ortiz, J. V.; Izmaylov, A. F.; Sonnenberg, J. L.; Williams-Young, D.; Ding, F.; Lipparini, F.; Egidi, F.; Goings, J.; Peng, B.; Petrone, A.; Henderson, T.; Ranasinghe, D.; Zakrzewski, V. G.; Gao, J.; Rega, N.; Zheng, G.; Liang, W.; Hada, M.; Ehara, M.; Toyota, K.; Fukuda, R.; Hasegawa, J.; Ishida, M.; Nakajima, T.; Honda, Y.; Kitao, O.; Nakai, H.; Vreven, T.; Throssell, K.; Montgomery, J. A., Jr.; Peralta, J. E.; Ogliaro, F.; Bearpark, M. J.; Heyd, J. J.; Brothers, E. N.; Kudin, K. N.; Staroverov, V. N.; Keith, T. A.; Kobayashi, R.; Normand, J.; Raghavachari, K.; Rendell, A. P.; Burant, J. C.; Iyengar, S. S.; Tomasi, J.; Cossi, M.; Millam, J. M.; Klene, M.; Adamo, C.; Cammi, R.; Ochterski, J. W.; Martin, R. L.; Morokuma, K.; Farkas, O.; Foresman, J. B.; Fox, D. J. Gaussian<sup>®</sup>16 Revision A.03. 2016; Gaussian Inc. Wallingford CT.
- (S2) TURBOMOLE V7.0 2015, a development of University of Karlsruhe and Forschungszentrum Karlsruhe GmbH, 1989-2007, TURBOMOLE GmbH, since 2007;

available from <http://www.turbomole.com>.

- (S3) Stein, T.; Kronik, L.; Baer, R. Reliable prediction of charge transfer excitations in molecular complexes using time-dependent density functional theory. *Journal of the American Chemical Society* **2009**, *131*, 2818–2820.
- (S4) Raeber, A. E.; Wong, B. M. The importance of short- and long-range exchange on various excited state properties of DNA monomers, stacked complexes, and Watson-Crick pairs. *Journal of Chemical Theory and Computation* **2015**, *11*, 2199–2209.
- (S5) Chai, J. D.; Head-Gordon, M. Long-range corrected hybrid density functionals with damped atom-atom dispersion corrections. *Physical Chemistry Chemical Physics* **2008**, *10*, 6615–6620.
- (S6) Borisevich, N. A.; Kazakov, S. M.; Kolesnik, E. E. ;; Kukhto, A. V.; Mit'kovets, A. I.; Murtazaliev, D. V.; Raichenok, T. F.; Khristoforov, O. V. Spectral-Luminescence Characteristics of Carbazole, Dibenzofuran, and Dinaphthofuran in the Gas Phase in Excitation by Electrons and Photons. *Journal of Applied Spectroscopy* **2001**, *68*, 871–876.
- (S7) Borisevich, N. A.; Povedailo, V. A.; Yakovlev, D. L. Fluorescence and fluorescence excitation spectra of jet-cooled carbazole. *Optics and Spectroscopy (English translation of Optika i Spektroskopiya)* **2006**, *100*, 351–356.
- (S8) Nguyen, D. D.; Trunk, J.; Nakhimovsky, L.; Spanget-Larsen, J. Electronic transitions of fluorene, dibenzofuran, carbazole, and dibenzothiophene: From the onset of absorption to the ionization threshold. *Journal of Molecular Spectroscopy* **2010**, *264*, 19–25.
- (S9) Zhang, S.; Qu, Z.; Tao, P.; Brooks, B.; Shao, Y.; Chen, X.; Liu, C. Quantum chemical study of the ground and excited state electronic structures of carbazole oligomers with

and without triarylborane substitutes. *Journal of Physical Chemistry C* **2012**, *116*, 12434–12442.

- (S10) Sun, C.; Ran, X.; Wang, X.; Cheng, Z.; Wu, Q.; Cai, S.; Gu, L.; Gan, N.; Shi, H.; An, Z.; Shi, H.; Huang, W. Twisted Molecular Structure on Tuning Ultralong Organic Phosphorescence. *Journal of Physical Chemistry Letters* **2018**, *9*, 335–339.
- (S11) Zhao, W.; Cheung, T. S.; Jiang, N.; Huang, W.; Lam, J. W.; Zhang, X.; He, Z.; Tang, B. Z. Boosting the efficiency of organic persistent room-temperature phosphorescence by intramolecular triplet-triplet energy transfer. *Nature Communications* **2019**, *10*.
- (S12) Wang, C. W.; Zhu, C.; Lin, S. H. Extremely solvent-enhanced absorbance and fluorescence of carbazole interpreted using a damped Franck-Condon simulation. *Journal of Chemical Physics* **2020**, *152*.
- (S13) Auty, A. R.; Jones, A. C.; Phillips, D. Spectroscopy and decay dynamics of jet-cooled carbazole and N-ethylcarbazole and their homocyclic analogues. *Chemical Physics* **1986**, *103*, 163–182.
- (S14) Bonesi, S. M.; Erra-Balsells, R. Electronic spectroscopy of N- and C-substituted chlorocarbazoles in homogeneous media and in solid matrix. *Journal of Luminescence* **2002**, *97*, 83–101.
- (S15) Ljubić, I.; Sabljić, A. CASSCF/CASPT2 and TD-DFT study of valence and rydberg electronic transitions in fluorene, carbazole, dibenzofuran, and dibenzothiophene. *Journal of Physical Chemistry A* **2011**, *115*, 4840–4850.
- (S16) Fornari, R. P.; Aragó, J.; Troisi, A. A very general rate expression for charge hopping in semiconducting polymers. *Journal of Chemical Physics* **2015**, *142*, 184105.

- (S17) Aragó, J.; Troisi, A. Regimes of Exciton Transport in Molecular Crystals in the Presence of Dynamic Disorder. *Advanced Functional Materials* **2016**, *26*, 2316–2325.
- (S18) Reimers, J. R. A practical method for the use of curvilinear coordinates in calculations of normal-mode-projected displacements and duschinsky rotation matrices for large molecules. *Journal of Chemical Physics* **2001**, *115*, 9103–9109.
- (S19) Bonesi, S. M.; Erra-Balsells, R. Electronic spectroscopy of carbazole and N- and C-substituted carbazoles in homogeneous media and in solid matrix. *Journal of Luminescence* **2001**, *93*, 51–74.
- (S20) Chakravorty, S. C.; Ganguly, S. C. Polarized Absorption Spectra of Carbazole Single Crystal. *The Journal of Chemical Physics* **1970**, *52*, 2760–2762.
- (S21) Chen, C.; Chi, Z.; Chong, K. C.; Batsanov, A. S.; Yang, Z.; Mao, Z.; Yang, Z.; Liu, B. Carbazole isomers induce ultralong organic phosphorescence. *Nature Materials* **2020**, 4–10.
- (S22) Levine, B. G.; Coe, J. D.; Martínez, T. J. Optimizing Conical Intersections without Derivative Coupling Vectors: Application to Multistate Multireference Second-Order Perturbation Theory (MS-CASPT2). *The Journal of Physical Chemistry B* **2008**, *112*, 405–413.
- (S23) Gao, X.; Bai, S.; Fazzi, D.; Niehaus, T.; Barbatti, M.; Thiel, W. Evaluation of Spin-Orbit Couplings with Linear-Response Time-Dependent Density Functional Methods. *Journal of Chemical Theory and Computation* **2017**, *13*, 515–524.